Advanced Fiber Materials
https://doi.org/10.1007/s42765-024-00481-x

RESEARCH ARTICLE

Bioactive Glass-Reinforced Hybrid Microfibrous Spheres Promote Bone Defect Repair via Stem Cell Delivery

Renjie Chen[1,2] · Yuanfei Wang[3] · Chenghao Yu[1,4,5] · Xiaopei Zhang[1,6] · Yawen Wang[1,6] · Tengbo Yu[4] · Tong Wu[1,6]

Received: 2 April 2024 / Accepted: 25 August 2024

Abstract

The development of biomimetic scaffolds that can promote osteogenic induction and vascularization is of great importance for the repair of large bone defects. In the present study, inorganic bioactive glass (BG) and organic polycaprolactone (PCL) are effectively combined by electrospinning and electrospray techniques to construct three-dimensional (3D) BG/PCL microfibrous spheres for the repair of bulk bone defects. The hybrid fibers, as well as the as-obtained 3D structure, can mimic the composition and architecture of native bone tissues. Furthermore, the BG/PCL microfibrous spheres show excellent biocompatibility and provide sufficient space and attachment sites for cell growth. The osteogenic differentiation of bone mesenchymal stem cells is also effectively facilitated when cultured on such hybrid microfibrous spheres. In vivo investigation utilizing rat femoral condyle bone defect models demonstrates that the BG/PCL microfibrous spheres loaded with bone mesenchymal stem cells can induce angiogenesis and promote the upregulation of bone-related protein expression, thus effectively facilitating bone regeneration at the defect site. The collective findings indicate that such BG/PCL hybrid microfibrous spheres have the potential to be effective carriers of stem cells. The microfibrous spheres loaded with stem cells have promising potential to be utilized as implantable biomaterials for the repair of bone defects.

Keywords Microfibrous spheres · Bone regeneration · Osteogenesis · 3D hybrid materials · Stem cell delivery

Renjie Chen and Yuanfei Wang have contributed equally to the work.

✉ Tengbo Yu
ytb8912@hotmail.com

✉ Tong Wu
twu@qdu.edu.cn

1 Medical Research Center, The Affiliated Hospital of Qingdao University, Qingdao University, Qingdao 266000, China

2 Beijing Jishuitan Hospital, Capital Medical University, Beijing 100035, China

3 Qingdao Stomatological Hospital Affiliated to Qingdao University, Qingdao 266001, China

4 Department of Orthopedic Surgery, Qingdao Municipal Hospital, University of Health and Rehabilitation Sciences, Qingdao 266071, China

5 Institute of Neuroregeneration and Neurorehabilitation, Department of Pathophysiology, School of Basic Medicine, Qingdao University, Qingdao 266071, China

6 Shandong Key Laboratory of Medical and Health Textile Materials, College of Textile and Clothing, Collaborative Innovation Center for Eco-Textiles of Shandong Province and the Ministry of Education, Qingdao University, Qingdao 266071, China

1 Introduction

Bone is the crucial organ of the human locomotor system, comprising an outer layer of cortical bone and an inner layer of cancellous bone [1, 2]. The primary constituents of bone are inorganic salts and collagen, which confer upon its considerable strength and resilience [5, 6]. In addition to providing protection and support for the human body, bones serve as attachment points for muscles and ligaments, enabling the realization of motor functions [3, 4]. Bone defects are usually caused by trauma, tumor removal, or bone infection, which seriously affect the patient's daily life and therefore require active treatment [7]. Currently, the most commonly employed clinical method is bone grafting, which entails the surgical implantation of autologous, allogeneic, or artificial bone into the defect site [8]. However, each of these methods has its inherent limitations. For instance, autogenous bone is only available in limited quantities and is, therefore, only suitable for small bone defects. Furthermore, additional surgical complications cannot be ruled out [9]. Allograft bone may result in rejection and is costly, while artificial bone is less biologically active and has a longer postoperative

Published online: 18 September 2024

recovery period. In these regards, it is, therefore, imperative to develop implantable bone repair materials for the treatment of bone tissue defects.

A wide variety of biomaterials have now been developed to promote bone tissue repair by loading various drugs or bioactive substances [10–25]. These materials include hydrogels [10–15], metal scaffolds [16–20], and microspheres [21–23]. Despite notable advancements in the application of these materials for bone regeneration, the challenge of repairing critical bone defects persists. The evidence indicates that stem cell therapies have a significant potential for promoting bone repair [11, 21]. Therefore, it is crucial to develop a material that can efficiently carry and deliver stem cells while maintaining their survival. Inspired by the composition of a native bone, a hybrid material composing organic and inorganic materials would be beneficial in preparing such a material. Among others, polycaprolactone (PCL) is an organic polymeric material with favorable mechanical properties, biocompatibility, and biodegradability, rendering it a commonly employed material in preparing biocompatible scaffolds [26–30]. Bioactive glass (BG) is an exciting inorganic material with the capacity to promote the osteogenic differentiation of stem cells, thereby having the potential to facilitate bone defect repair [31–34]. The combination of these two components to prepare three-dimensional (3D) materials that mimic the structure of natural extracellular matrix for the delivery of stem cells has the potential to facilitate the rapid repair of significant bone defects.

In the present study, we designed and fabricated a class of BG/PCL (BP) microfibrous spheres using electrospinning and electrospray techniques. The resulting 3D fibrous and honeycomb structures exhibited biomimetic architecture of native bone tissue [35–38]. In addition to the focus on the material composition and structure, injectability is also a key consideration when developing materials for bone regeneration [24, 25, 35–38]. To achieve the injectability and fixability of the bone defect site, gelatin methacryloyl (GelMA), which has suitable biological and light-curing properties, was chosen as the carrier for delivering microfibrous spheres [39–42]. As such, the BP microfibrous spheres developed in this study exhibited an optimal structural configuration while containing osteogenically active substances. Their injectability afforded distinctive advantages in bone regeneration applications. The biocompatibility of the spheres was then verified by live/dead cell staining. The osteogenic differentiation ability was determined using alkaline phosphatase (ALP) assay and real-time quantitative polymerase chain reaction (RT-qPCR). In vivo investigation was carried out to repair bone defects using rat femoral condyle defect models (Scheme 1). Micro-computed tomography (micro-CT) and histological staining were employed to assess the efficacy of bone regeneration. The findings demonstrated that such BP microfibrous spheres exhibited a robust capacity to sustain stem cell viability and facilitate their delivery to the defect sites for the purpose of facilitating bone repair.

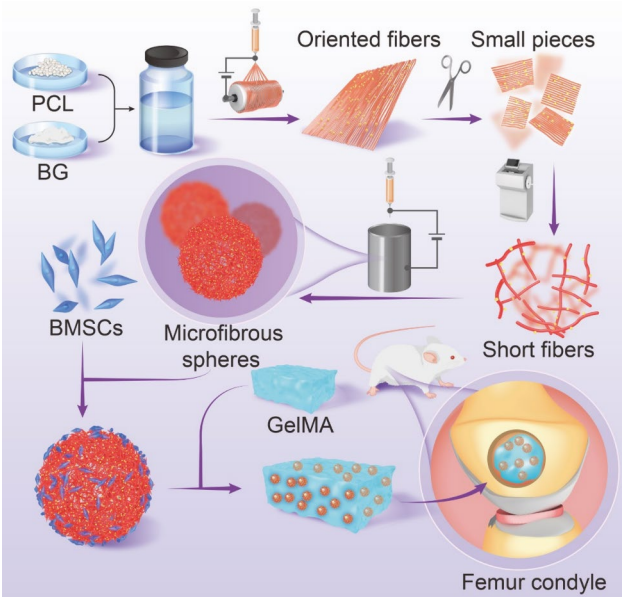

Scheme 1 Schematic diagram showing the fabrication of BP microfibrous spheres and their use in repairing femoral condylar bone defects in rats by combining the therapy of BMSCs

2 Experimental Section

2.1 Preparation and Characterization of Oriented BP Fibers

A solution of PCL (Sigma, Germany) hexafluoroisopropanol (Wengjiang, China) with a concentration of 10 wt.% was initially prepared, and BG (Vofor, China) was added to the PCL solution and stirred overnight. Subsequently, the aforementioned solution was drawn up with a 5 mL syringe and subjected to spinning using an electrospinning device (ET-2535H, Ucalery Technology, China). The spinning parameters were as follows: flow rate of 1 mL/h, roller speed of 2800 rpm, receiver distance of 15 cm, and voltage (DC) of 16 kV. Subsequently, the collected fibers were observed using a field emission scanning electron microscope (FE-SEM, Regulus8100, HITACHI, Japan). The diameters of the fibers and BG were measured using the ImageJ software.

2.2 Preparation and Characterization of BP Microfibrous Spheres

The collected fibers were segmented into small pieces of equal size (1 cm × 1 cm). Then the fibers were cut into short fibers of 50 μm in length using a freezing microtome (Leica, Germany) in a direction perpendicularly to the long axis of the fibers. After repeated centrifugation and resuspension, the short fibers were homogeneously dispersed in a gelatin aqueous solution (0.3 wt%). The BP microfibrous spheres were prepared using the electrospinning device described above. A metal cup filled with liquid nitrogen served as the receiving device. The preparation parameters were as follows: flow rate of 30 mL/h, voltage (DC) of 6–10 kV. The collected microfibrous spheres were frozen overnight in a − 80 °C refrigerator and then dried in a freeze dryer (Christ, Germany) for 48 h.

The surface morphology of the microfibrous spheres was observed using FE-SEM. The mechanical properties of the microfibrous spheres were evaluated using the Instron 330 universal testing system. The diameter of the microfibrous spheres was recorded, and then they were subjected to compression at a constant compression rate of 1 mm/min. The experiments were terminated when the shape variable reached 30%. The compressive modulus of the microfibrous spheres was calculated from the stress–strain curve. The chemical composition of the microfibrous spheres was characterized by Fourier transform infrared spectroscopy (FT-IR) with a resolution of 4 cm^{-1}.

2.3 Cell Culture

Bone mesenchymal stem cells (BMSCs, Hycyte, China) were cultured in BMSCs growth medium (Hycyte, China). The medium was supplemented with 10% fetal bovine serum (FBS, Gibco, USA), 1% penicillin/streptomycin (Hycyte, China), and 1% glutamine (Hycyte, China). Human umbilical vein endothelial cells (HUVECs, Hycyte, China) were cultured in a specialized medium (Hycyte, China). All cells were cultured at 37 °C and 5% CO_2 conditions, and the medium was refreshed every 2 days.

2.4 Biocompatibility Assessment of BP Microfibrous Spheres

BMSCs were inoculated onto sterilized BP microfibrous spheres at a density of 1×10^4 cells per well and cultured using BMSCs growth medium. After 3 and 7 days of culture, the cells were stained using a live/dead cell staining kit (MeilunBio, Dalian, China) and observed under a confocal microscope (STELLARIS5, Leica). The number of live and dead cells in the fluorescence images was detected using ImageJ software, and the cell survival rate was calculated. The morphology and spreading of BMSCs on the spheres were observed by FE-SEM on day 3.

2.5 Osteogenic Differentiation Capacity of BMSCs on BP Fibers

The fibers with different BG content were trimmed to the appropriate size and then attached to the circular glass sheets with bio-glue. BMSCs were inoculated on the BP fibers and cultured in a 24-well plate with a density of 1×10^5 cells per well. 1 mL of BMSCs growth medium was added to each well for co-cultivation. After culturing with BMSCs growth medium for 24 h, the medium was replaced by BMSCs osteogenic differentiation complete medium (Hycyte, China). The cells on the BP fibers were stained with the ALP staining kit (Solarbio, Beijing, China) on days 7 and 21 and observed under the optical microscope (Ni-U, Nikon, Japan). The method for measuring ALP activity was derived from previous literature [43].

2.6 Osteogenic Gene Expression in BMSCs Inoculated on BP Microfibrous Spheres

BMSCs were co-cultured with sterilized BP microfibrous spheres at a density of 2×10^5 cells per well in 24-well plates. Following a 24-h incubation period with BMSCs growth medium, the medium was replaced with BMSCs osteogenic differentiation complete medium. The cultural conditions were the same as described previously. On days 7 and 14 of the culture, the cells on spheres were digested with trypsin, and RNA was extracted using the total RNA extraction kit (Vazyme, Nanjing, China). The expression of each osteogenic gene was then detected using a one-step RT-qPCR kit (ABclonal, Wuhan, China) ($n = 3$). The relative expression of genes was based on the housekeeping gene GAPDH (Table S1, Supporting information). The RT-qPCR primers were synthesized by Sangon Biotech (Shanghai) Co., Ltd.

2.7 Angiogenesis and Mineralization Experiments

In the angiogenesis test, Matrigel (Solarbio, Beijing, China) was initially gelatinized in the 24-well plate, and 2×10^4 HUVECs were subsequently seeded in each well. A solution of 200 μL of the extraction liquid or phosphate buffer solution (PBS, control group) was mixed with 800 μL of the medium for HUVECs culture. The extraction liquids were obtained by soaking microfibrous spheres with different BG contents in PBS for 24 h. HUVECs were observed after 3

and 6 h under the optical microscope. The node number and total tube length of each group were analyzed using the ImageJ software. The mineralization of the spheres was assessed using simulated body fluid (SBF, Solarbio, Beijing, China). The spheres and fibers were immersed in the 2× SBF solution for mineralization, and their morphology was observed by FE-SEM on days 1, 4, and 7 of soaking.

2.8 Construction of Rat Femoral Condyle Defect Model

A total of 60 male Sprague–Dawley (SD) rats (8 weeks, 280–320 g) were randomly divided into 6 groups: sham, control, GelMA, GelMA with BMSCs (GelMA-B), GelMA with microfibrous spheres (GelMA-M), and GelMA with the microfibrous spheres loaded with BMSCs (GelMA-MB). The rats were anesthetized by intraperitoneal injection of 3% pentobarbital sodium (35 mg/kg). The hair surrounding the knee joint was shaved, and the skin was disinfected with iodophor sanitizer. The subcutaneous tissue was then peeled off, exposing the femoral condyles. A cylindrical defect, measuring approximately 4 mm in depth and 3.5 mm in diameter, was created in the femoral condyle using a high-speed electric drill [41, 42]. The wound was then sutured layer by layer, and antibiotics were used for the first 3 days after surgery to prevent infection. In the sham group, only the skin and subcutaneous tissue were dissected, and no bone defect was created. In the control group, bone defects were created without filling. In the GelMA, GelMA-B, GelMA-M, and GelMA-MB groups, bone defects were created and filled with GelMA, a mixture of GelMA and BMSCs, a mixture of GelMA and BP microfibrous spheres, and a mixture of GelMA and BP microfibrous spheres loaded with BMSCs, respectively. The number of BMSCs in the GelMA-B and GelMA-MB groups was 1×10^7. All animal experiments were approved by the Animal Ethics Committee of Qingdao University (No. 20220624SD7220230110086).

2.9 Micro-CT Evaluation of Bone Defect Repair

At weeks 4 and 8 post-surgery, five rats were sacrificed in each group, and samples of femoral condyles were obtained and fixed in 4% paraformaldehyde (Biosharp, China) for 24 h. The femoral condyles were scanned using micro-CT (GX2, PerkinElmer, Japan). The bone tissue volume/total tissue volume (BV/TV) at the defect site was calculated for each specimen using CTAn software [44].

2.10 Histological Evaluation of Bone Defect Repair

The femoral condyles obtained from the experiments above were immersed in ethylenediaminetetraacetic acid (EDTA) decalcified solution (Leagene, China) for 1 month. The EDTA decalcified solution was replaced every 7 days. The decalcified femoral condyles were dehydrated and paraffin-embedded, resulting in the preparation of 5-μm thick sections. The sections were examined using staining techniques, including hematoxylin and eosin (H&E), Masson's trichrome, and immunohistochemistry (IHC). The primary antibodies utilized for IHC were RUNX2 (Bioss, China), CD31(Abcam, US), and OCN (Bioss, China).

2.11 Statistical Analysis

All tests in this study were repeated at least three times, and the results were presented as mean ± standard deviation. The Student *t* test was used to compare the differences between two groups, and one-way analysis of variance (ANOVA) was used to compare the differences between multiple groups. $P < 0.05$ indicated that the differences were statistically significant. *, **, ***, and ns represented $P < 0.05$, $P < 0.01$, $P < 0.001$, and $P > 0.05$, respectively.

3 Results and Discussion

3.1 Preparation and Characterization of the BP Microfibrous Spheres

As shown in Fig. 1a and b, the oriented PCL fibers loaded with BG were successfully prepared with a uniform distribution of BG within the fibers. The surface of the BP microfibrous spheres exhibited a porous and rough structure (Fig. 1c and d), which increased the surface area of the spheres and provided additional adhesion sites for the cells [45]. The sphere size ranged from 1 to 5 mm and decreased accordingly with increasing applied voltage (Fig. 1e). The mean diameters of BG particles in the 1%, 2%, and 3% BP fibers were (0.79 ± 0.38), (0.81 ± 0.30), and (0.82 ± 0.50) μm, respectively, with no significant difference (Fig. 1f). The mean diameters of pure PCL and 1%, 2%, and 3% BP fibers were (1.11 ± 0.27), (1.13 ± 0.35), (1.09 ± 0.22), and (1.05 ± 0.26) μm, respectively, with no significant difference (Fig. 1g).

The stress–strain curve and compression modulus of spheres with different BG contents demonstrated that the incorporation of BG did not alter the mechanical properties of the spheres (Fig. S1a-b). Appropriate mechanical strength is conducive to the conduction of force by bones and contributes to bone regeneration [15]. The FT-IR spectra of the different groups are presented in Fig. S1c. The peaks at 1463 cm^{-1}, 2860 cm^{-1}, and 2950 cm^{-1} indicated the presence of CH_2, while the peak at 1642 cm^{-1} indicated the presence of C = O, thus confirming the presence of PCL [15, 29]. The peaks at 1540 cm^{-1} and 1232 cm^{-1} indicated the presence of amides, confirming the incorporation of gelatin. With the exception of the spheres lacking BG, the remaining

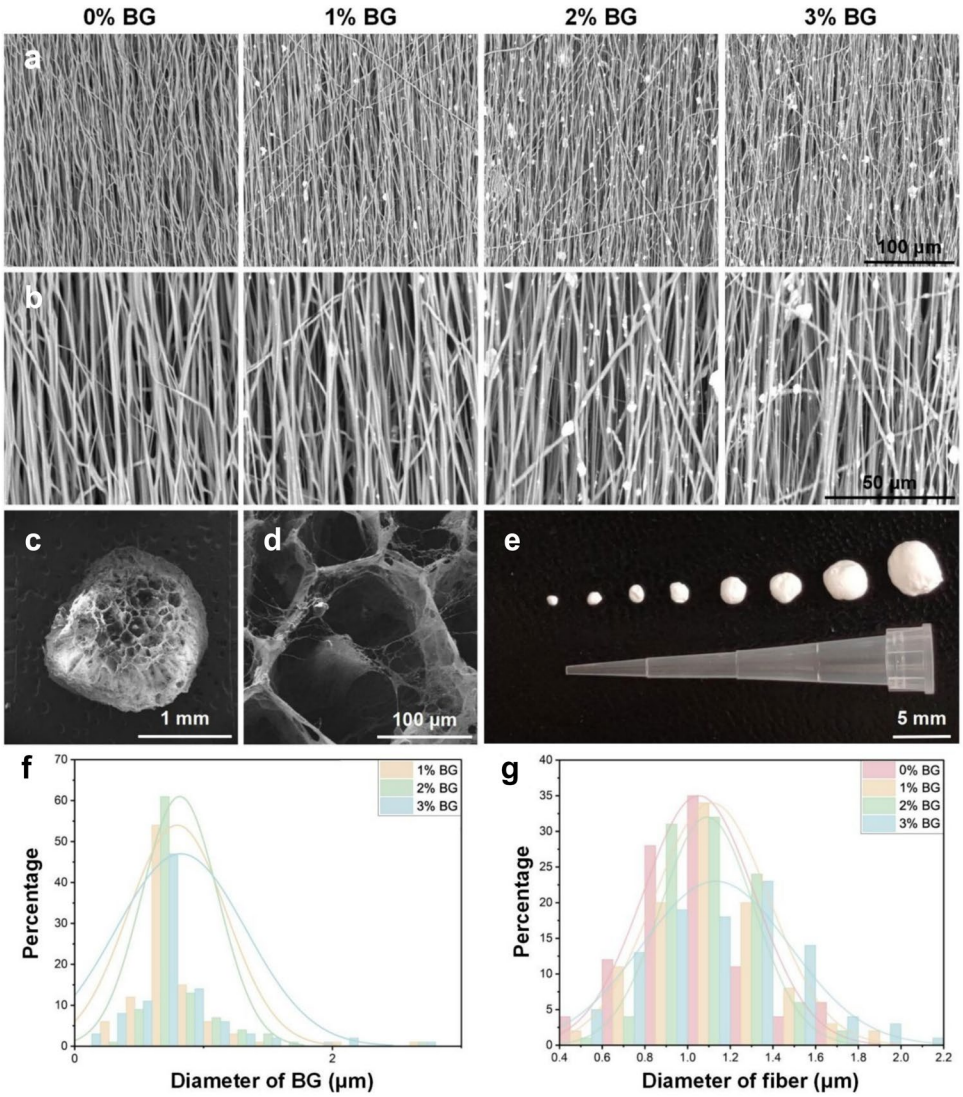

Fig. 1 Characterization of different fibers and BP microfibrous spheres. **a**, **b** SEM images of fibers with 0%, 1%, 2%, and 3% BG at **a** ×1000 or **b** ×3000 field of view. **c**, **d** SEM images of the BP microfibrous spheres containing 2% BG. **e** Photographs of BP microfibrous spheres of different sizes. **f** Histogram of the size distribution of BG particles in different BP fibers. **g** Histogram of the size distribution of pure PCL and different BP fibers

three groups exhibited peaks at 960 cm^{-1}, indicative of the Si element. This observation suggests that the introduction of BG was successful [10].

3.2 Biocompatibility Assessment of the BP Microfibrous Spheres

Although all raw materials were nontoxic, it was imperative to ascertain the biocompatibility of the microfibrous spheres prior to their utilization in subsequent experiments. (Fig. 2). On day 3, the survival rate of cells in all groups exceeded 84%, with no significant difference between the groups. On day 7, the cells proliferated in all groups, with cell survival rates exceeding 95%. The results demonstrated that the BP microfibrous spheres exhibited low cytotoxicity, while the BMSCs showed robust proliferative ability. SEM images revealed that the BMSCs exhibited extensive spreading on the spheres with a spindle shape, indicating optimal conditions (Fig. S2).

3.3 Osteogenic Differentiation of BMSCs on BP Fibers and Microfibrous Spheres

ALP staining was employed to assess the osteogenic differentiation capacity of BMSCs on different BP fibers [43]. Following a 7-day osteogenic differentiation period, the ALP activity in the 2% BG group was significantly higher than in the other groups. Furthermore, the ALP activity in the 1%

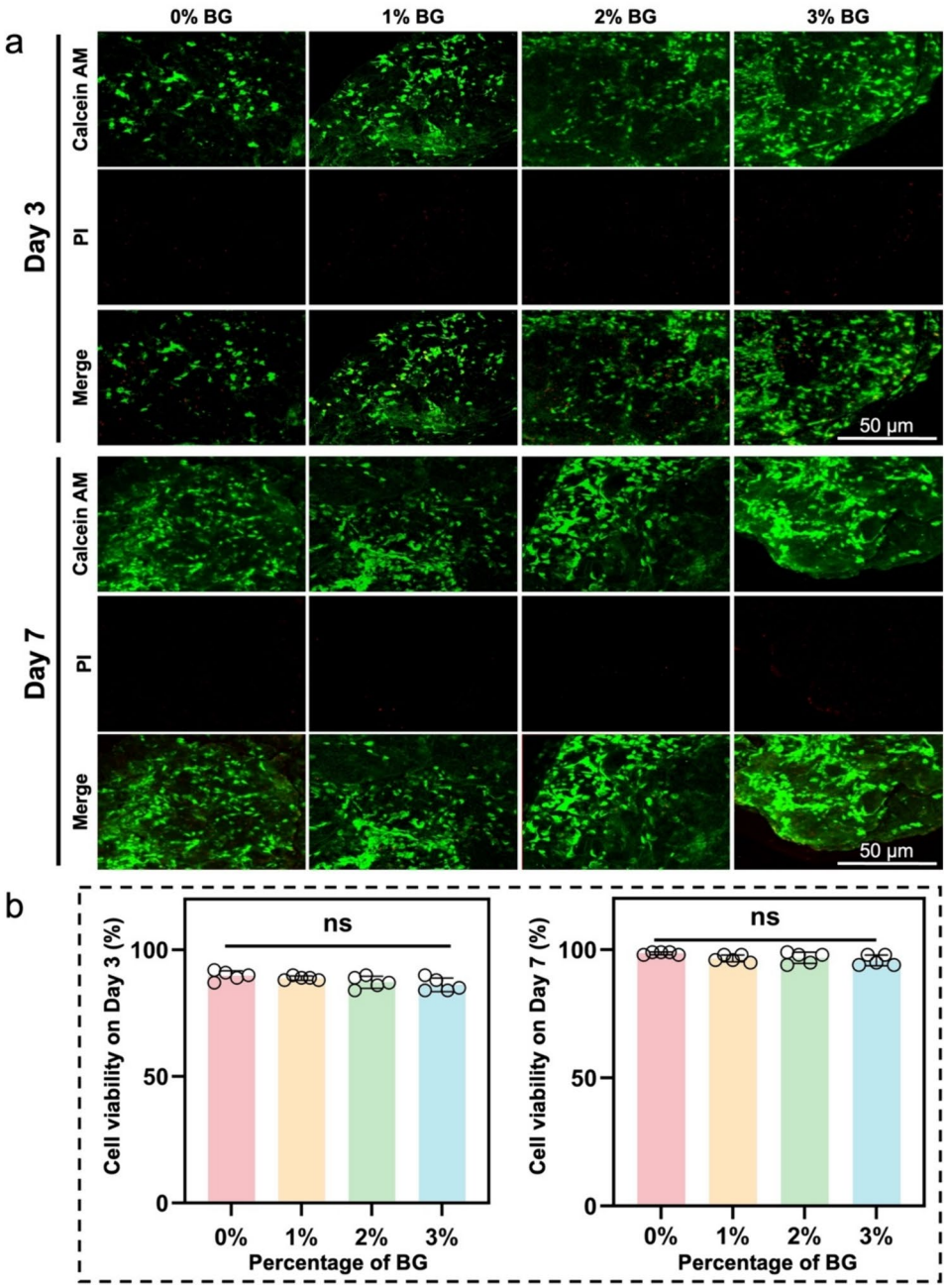

Fig. 2 Biocompatibility assessment of the BP microfibrous spheres. **a** Live/dead staining micrographs and **b** cell survival rates after culturing BMSCs on the different BP microfibrous spheres for 3 and 7 days. "ns" indicates no significant difference between the groups

BG group was significantly higher than that observed in the 0% BG group (Fig. 3a, b). Following 21 days of osteogenic differentiation, a significant increase in ALP activity was observed in all groups. Nevertheless, the ALP activity of the 2% BG group remained markedly elevated in comparison to the other groups, suggesting that BMSCs in the 2% BG group demonstrated a more pronounced capacity for osteogenic differentiation.

To further evaluate the osteogenic differentiation of BMSCs on different microfibrous spheres, RT-qPCR was used to assess the expression of three common osteogenic genes: ALP, OPN, and RUNX2 [46]. The ALP gene is associated with osteogenic differentiation of stem cells, the OPN gene can effectively regulate osteoclast activity, and the RUNX2 gene plays an important role in inducing the differentiation of immature osteocytes into mature osteoblasts [46, 47]. In this assay, BMSCs were inoculated on the different microfibrous spheres under osteogenic induction conditions. On day 7, the expression of the OPN gene was significantly greater in the 2% BG group, and the expression of ALP and

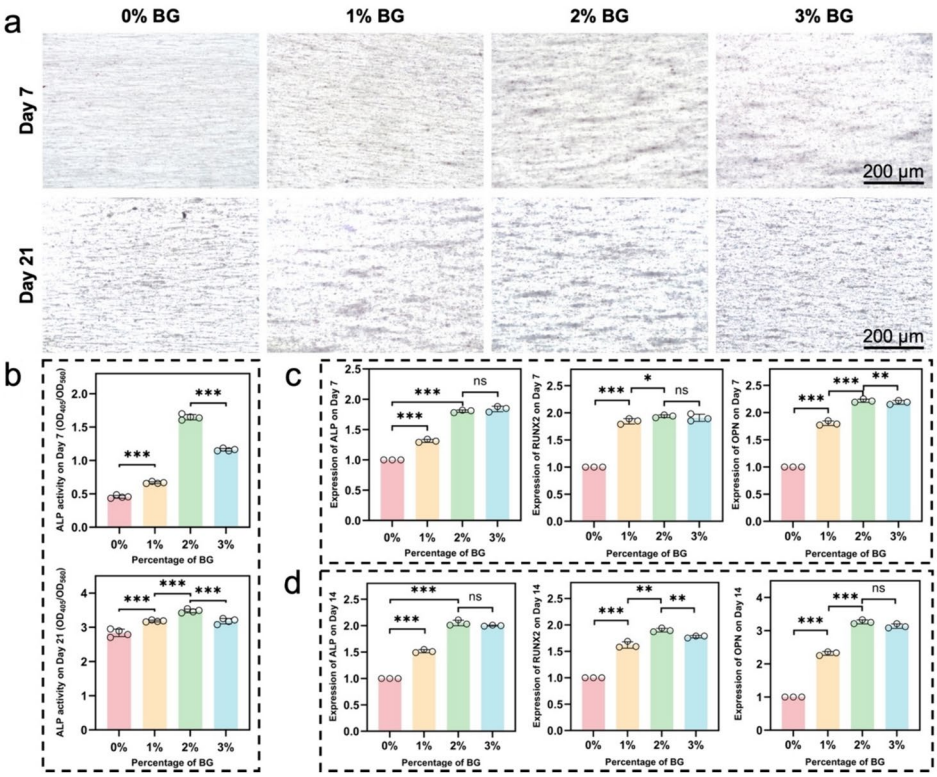

Fig. 3 The osteogenic differentiation capability of BMSCs on different BP fibers and microfibrous spheres. **a** ALP staining micrographs and **b** quantitative analysis of ALP activity after culturing BMSCs on different fibers for 7 and 21 days. **c**, **d** Gene expression of ALP, RUNX2, and OPN after culturing BMSCs on different BP microfibrous spheres for **c** 7 and **d** 14 days. "ns" indicates no significant difference between the groups. $*P<0.05$, $**P<0.01$, and $***P<0.001$ indicate that the differences between the compared groups are statistically significant

RUNX2 was significantly greater than that observed in the 0% and 1% BG groups. Nevertheless, no statistically significant difference was identified between the 2% and 3% BG groups (Fig. 3c). On day 14, the RUNX2 gene expression in the 2% BG group was found to be significantly greater than that in the other groups. In comparison, the ALP and OPN expression was significantly greater than that in the 0% and 1% BG groups (Fig. 3d). No statistically significant difference was observed between the 2% and 3% BG groups. These results demonstrated that 2% BP microfibrous spheres exhibited the most remarkable ability to induce osteogenic differentiation of BMSCs. Consequently, the microfibrous spheres containing 2% BG were employed for subsequent in vivo investigations.

3.4 In Vitro Evaluation of Angiogenesis and Mineralization

Angiogenesis is a critical process in the repair of bone defects. The formation of new blood vessels can facilitate the migration, secretion, and infiltration of undifferentiated stem cells into the scaffold, thereby promoting bone regeneration [8, 41]. The angiogenesis test revealed that the 2% and 3% BG groups exhibited enhanced tube formation after 3 and 6 h, respectively. However, no discernible difference was observed between the two groups in terms of node numbers and tube length (Fig. S3). In addition, the BP fibers and microfibrous spheres containing 2% BG were employed to investigate mineralization (Fig. S4). The results demonstrated that, following 1 day, mineralized particles had formed on both the fibers and microfibrous spheres. This mineralization process was observed to continue over time.

3.5 Micro-CT Observation After Bone Repair Using the BP Microfibrous Spheres

Based on the results of in vitro experiments, 2% BP microfibrous spheres were selected for use to repair femoral defects in rats. The animal experiment was divided into six groups: sham, control, GelMA, GelMA-B, GelMA-M, and GelMA-MB. A 3.5-mm rat femoral defect was initially prepared, and the prepared material was subsequently injected into the defect site (Fig. S5). The results demonstrated that the injected materials were effectively integrated within the surrounding bone tissues (Video S1, Supporting information). The rats were sacrificed at 4 and 8 weeks post-surgery,

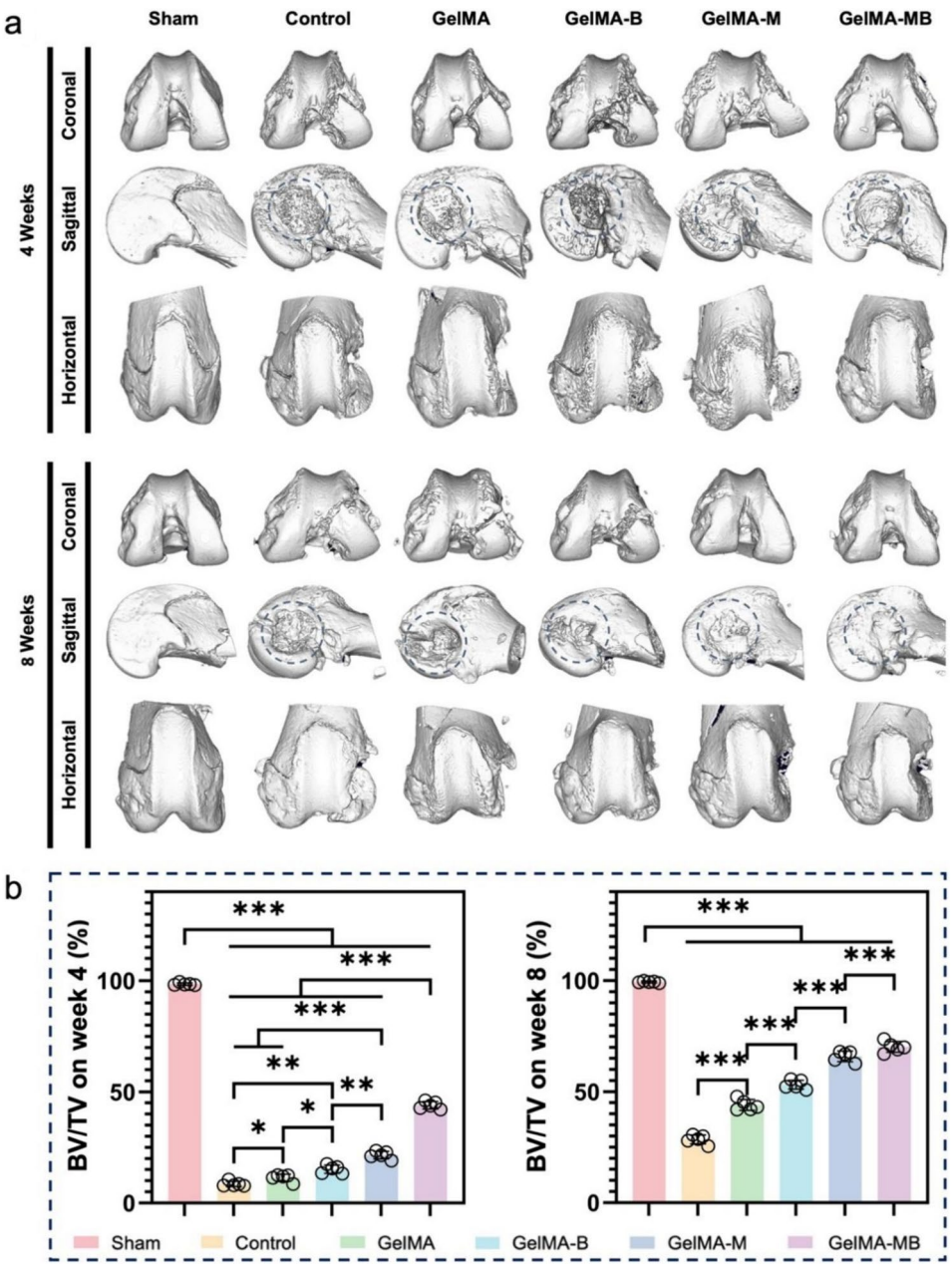

Fig. 4 **a** Micro-CT micrographs showing the osteogenic capacity of the different groups using rat femoral condyle defect models at weeks 4 and 8 post-surgery. **b** BV/TV values of each group at weeks 4 and 8. * $P<0.05$, ** $P<0.01$, and *** $P<0.001$ indicate significant differences between comparison groups

and the femurs were scanned and 3D reconstructed using micro-CT (Fig. 4a). For enhanced visualization, the areas of bone defects were marked with dashed boxes on the sagittal images. Bone defect modeling was not conducted in the sham group, and thus this group was employed as the standard for comparison. At 4 weeks post-surgery, fractures occurred at the molding site in all groups except the sham and GelMA-MB groups. Moreover, none of the BV/TV values (representing the volume of newly formed bone) exceeded 25%, with the exception of the GelMA-MB group (Fig. 4b). At 8 weeks post-surgery, fractures were observed at the injured sites in the control, GelMA, and GelMA-B groups. These fractures may be related to the unfixed knee after surgery. The filling materials may provide sufficient mechanical support, and the introduction of BMSCs further augmented the mechanical strength of BP microfibrous spheres. As a result, no fractures were observed in the GelMA-MB group. The findings revealed

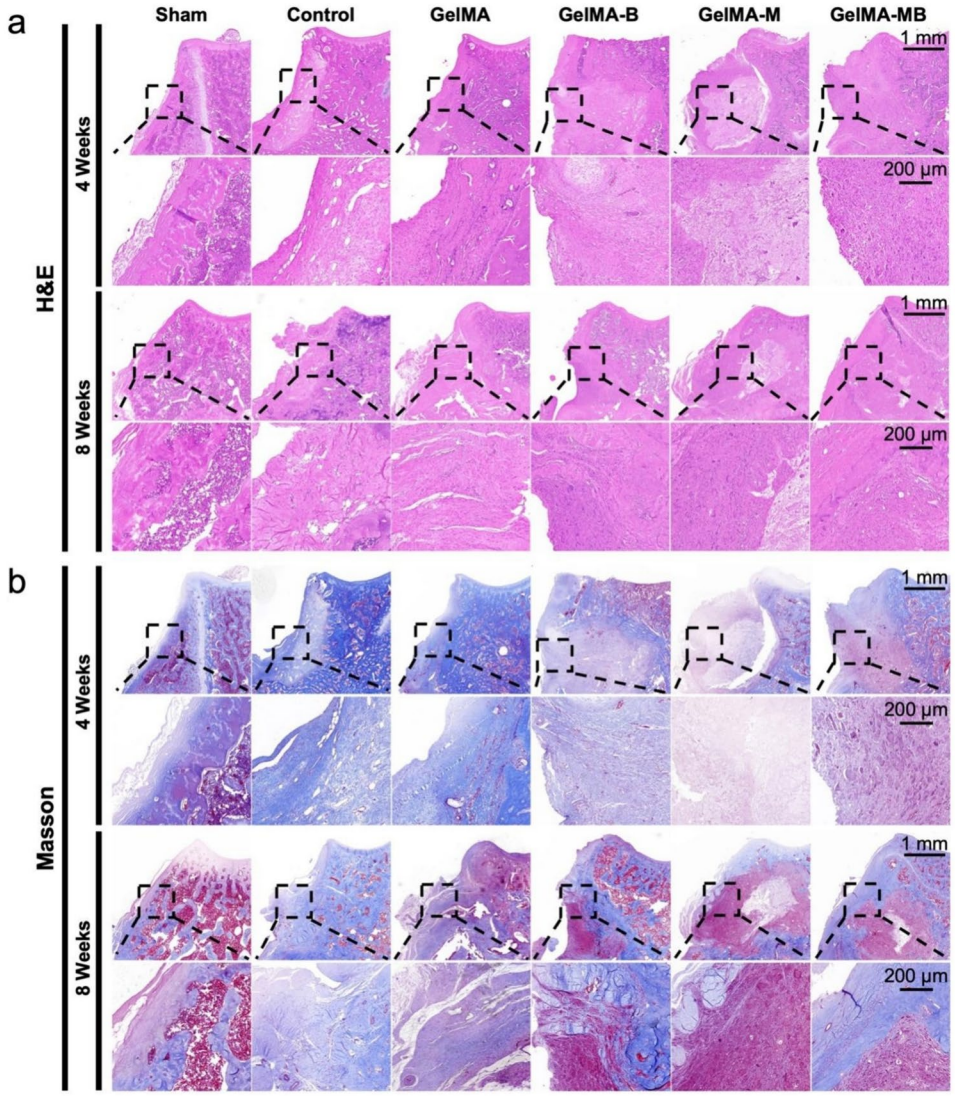

Fig. 5 **a** H&E and **b** Masson's trichrome staining micrographs showing the osteogenic capacity of the different groups using rat femoral condyle defect models at weeks 4 and 8 post-surgery

that the GelMA-MB group demonstrated the most substantial repair outcomes, followed by the GelMA-M group, the GelMA-B group, the GelMA group, and finally, the control group. The results indicated that GelMA, BMSCs, and BP microfibrous spheres have the potential to facilitate bone defect repair. Among the various components, the BP microfibrous spheres exhibited the most pronounced effect on augmenting the mechanical strength of the defect site while creating a conducive environment for the osteogenic differentiation of BMSCs. This ultimately led to a more effective promotion of bone defect repair. By week 8, the BV/TV value of the GelMA-MB group had exceeded 50%, a notable improvement over previous studies where the BV/TV value of the experimental groups did not exceed 40% [41, 42]. This provides further evidence that BP microfibrous spheres prepared in this study are effective in repairing bone defects.

3.6 Histological Evaluation After Bone Repair Using the BP Microfibrous Spheres

To further evaluate the effect of microfibrous spheres on bone formation in vivo, histological analysis was conducted on specimen sections using H&E and Masson's trichrome staining (Figs. 5 and S6). At week 4, the control group exhibited the formation of a single layer of fibrous tissue in the defect area. In contrast, the GelMA group demonstrated the generation of more newly formed tissue, although it remained predominantly fibrous. The observation of a limited number of new capillaries in the GelMA-B group may

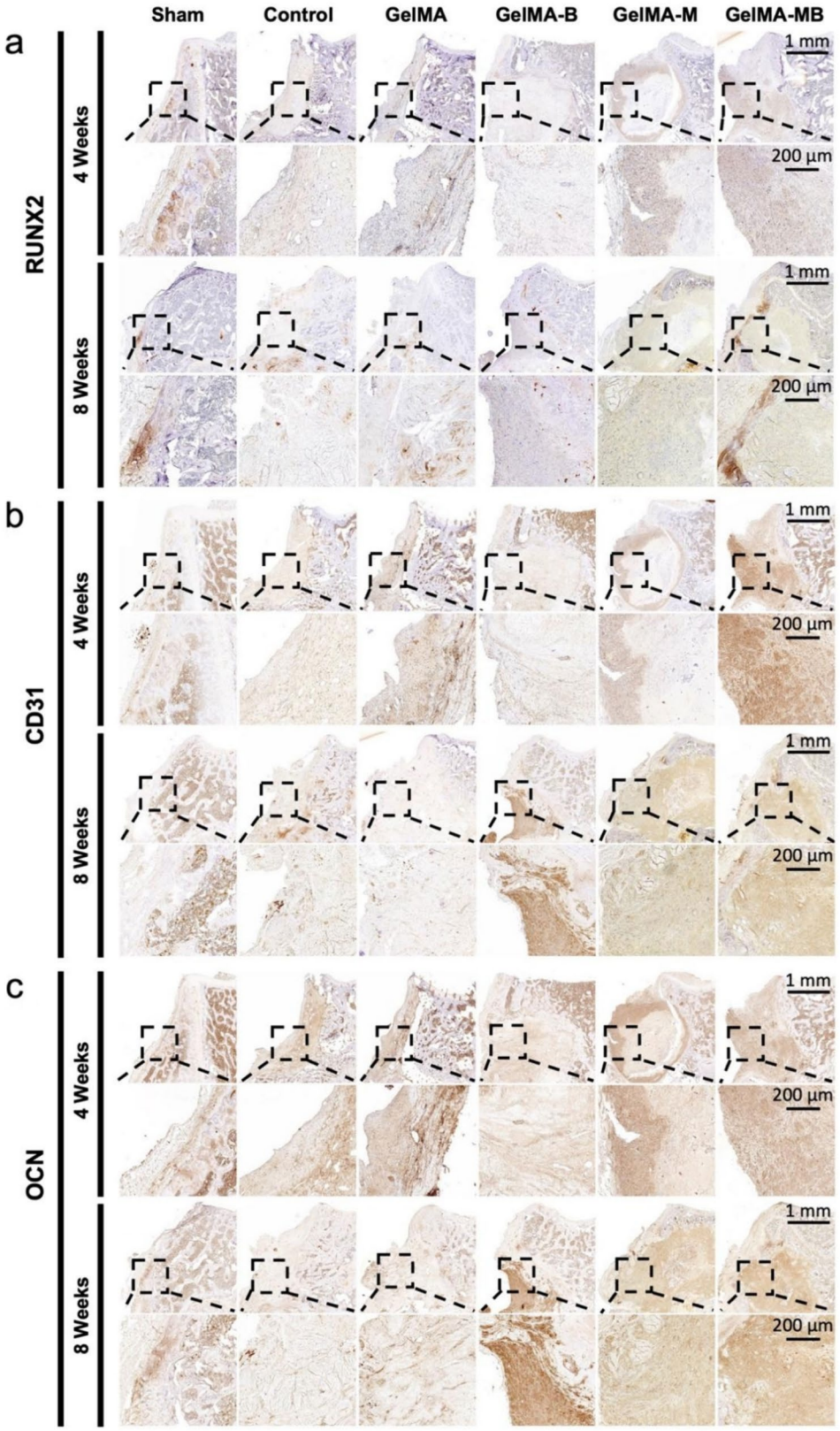

Fig. 6 IHC staining micrographs showing the osteogenic capacity of the different groups using rat femoral condyle defect models at weeks 4 and 8 post-surgery: **a** RUNX2, **b** CD31, **c** OCN

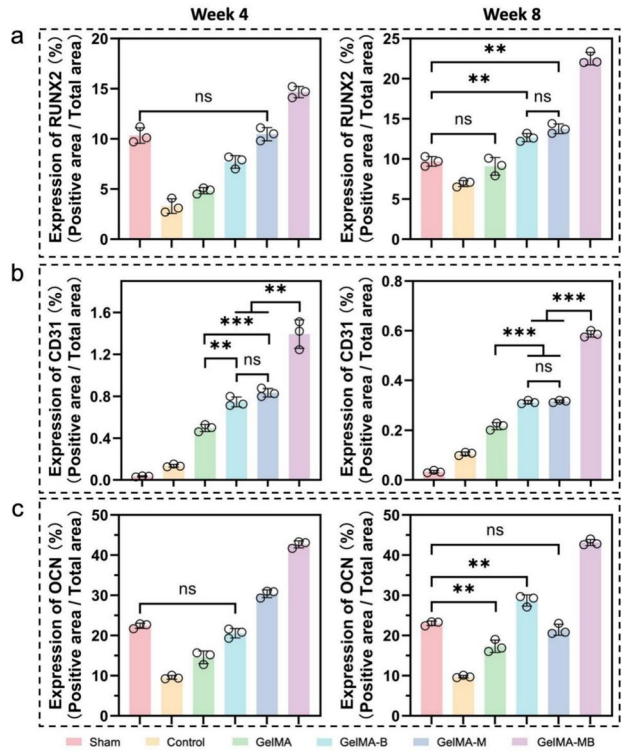

Fig. 7 Quantitative analysis of **a** RUNX2-, **b** CD31-, and **c** OCN-positive regions using the IHC staining micrographs in Fig. 6. "ns" indicates no significant difference between the groups. ** $P<0.01$ and *** $P<0.001$ indicate that the differences between the compared groups are statistically significant

indicate the initiation of new bone formation. The GelMA-M and GelMA-MB groups demonstrated incomplete degradation of residual microfibrous spheres. Nevertheless, the GelMA-MB group exhibited a reduction in residual fibers and an increase in neovascularized capillaries, which may be attributed to the acceleration of the process by BMSCs. In the H&E and Masson's trichrome stained images at week 8, it was observed that the defect areas were still evident in the control, GelMA, and GelMA-B groups. Notably, all the defects exhibited significant angiogenesis, with the GelMA-MB group demonstrating the most pronounced outcomes. It is evident that both the GelMA-M and GelMA-MB groups exhibited the formation of bone tissues. Furthermore, the newly formed bone structure in the GelMA-MB group exhibited a greater degree of similarity to that of a normal bone.

Furthermore, the expression of RUNX2, CD31, and OCN proteins was investigated following the implantation of different samples into the bone defect sites for 4 and 8 weeks through IHC staining (Fig. 6). The expression levels of RUNX2, CD31, and OCN were found to be significantly greater in the GelMA-MB group (Fig. 7), exhibiting a pattern of results comparable to those observed in the previous analyses. Among them, RUNX2 has been linked to osteoblast differentiation. At week 4, no statistically significant difference in RUNX2 expression was observed between the GelMA-M and sham groups. At week 8, the samples treated with GelMA-B and GelMA-M exhibited significantly elevated levels of RUNX2 expression compared to the sham group. Nevertheless, no significant difference was observed between the two groups. The expression level of RUNX2 in the GelMA-MB group was higher than that observed in the GelMA-M and GelMA-B groups. The findings suggest that BMSCs and microfibrous spheres demonstrate comparable capacity to contribute to bone differentiation, with the concomitant use of both significantly enhancing this effect. CD31 is associated with neovascularization, which has been shown to facilitate osteogenesis [46]. The expression of CD31 in the GelMA-B and GelMA-M groups was not found to differ significantly. However, the outcomes were superior to those observed in the GelMA group at both 4 and 8 weeks, indicating that BMSCs and the microfibrous spheres are actively involved in promoting angiogenesis. The expression level of CD31 in the GelMA-MB group was significantly higher than that observed in all other groups. At week 8, the expression level of CD31 in the GelMA-MB group was more than fivefold higher than in the control group. These findings are consistent with those of previous research [42]. The expression of OCN has been demonstrated to correlate with the deposition of bone matrix [48]. At 4 weeks post-surgery, no statistically significant difference in OCN expression was observed between the GelMA-B and sham groups. However, in week 8, the GelMA-B group exhibited significantly greater OCN expression than the sham group. In contrast, the GelMA-M group exhibited an inverse trend at these two time points. The microfibrous spheres and BMSCs each played a significant role in bone matrix deposition during the initial 4-week period and subsequent 4-week period. The expression level of OCN in the GelMA-MB group was significantly greater than observed in the other groups. At week 8, the OCN expression level in the GelMA-MB group was also significantly higher than that observed in the experimental groups in the previous study [49]. These findings demonstrate that combining microfibrous spheres with BMSCs represents an efficacious strategy for stimulating angiogenesis and osteogenic gene expression, which collectively facilitate the expeditious repair of bone defects.

The results of the in vivo experiments demonstrated that the GelMA-MB group exhibited the most notable capacity for bone defect repair. Furthermore, the bone regeneration potential of both the GelMA-B and GelMA-M groups was observed to be superior to that of the GelMA group. The results demonstrate that both microfibrous spheres and BMSCs contributed to the repair of bone defects, with

the combination of these factors resulting in a notable enhancement in bone regeneration. A comparison of micro-CT results in experimental groups with previous studies using the same animal model also indicated that the BP microfibrous spheres loaded with BMSCs could facilitate bone defect repair [41, 42]. In tissue engineering, spheres have been extensively employed as carriers for stem cells [21, 41, 42]. The BP microfibrous spheres developed in this study not only served as cell carriers but also mimicked the tissue structure of bone, providing space for stem cell recruitment and inducing their osteogenic differentiation. This approach represents a novel option for the repair of bone defects in the clinic. Although the present study preliminarily demonstrated the positive effects of BP microfibrous spheres in repairing bone defects, further investigation is required to address some limitations. For example, the diameter of the microfibrous spheres could be reduced, which would facilitate the attainment of a greater specific surface area and a more efficient injection rate. It is anticipated that the utilization of microfibrous spheres with osteogenic-inducing capabilities will result in enhanced clinical outcomes for patients with bone defects.

4 Conclusion

In this study, we employed advanced electrospinning and electrospray technologies to successfully develop a class of BP microfibrous spheres. The spheres exhibited excellent biocompatibility, a surface structure conducive to cell adhesion, and the capacity to enhance the expression of osteoblastic genes. In addition, the BP microfibrous spheres demonstrated robust angiogenic and mineralization ability in vitro. Furthermore, they exhibited suitability as carriers for stem cells. In a rat femoral defect model, BP microfibrous spheres loaded with BMSCs demonstrated substantial improvements in both angiogenesis and osteogenic differentiation, as well as promoting the healing of bone defects. These findings suggest that this approach may represent a highly promising new avenue for the treatment of clinically significant bone defects.

Supplementary Information The online version contains supplementary material available at https://doi.org/10.1007/s42765-024-00481-x.

Acknowledgements This research was supported by Special Funds for Taishan Scholars Project of Shandong Province (No. tsqn202211125), Natural Science Foundation of Shandong Province (ZR2021YQ17), National Natural Science Foundation of China (82001970), Young Elite Scientists Sponsorship Program by CAST (No. YESS20200097), Shandong Province key research and development support project (2021SFGC0502), Qingdao Key Health Discipline Development Fund (2022-2024), Qingdao Clinical Research Center for Oral Diseases (22-3-7-lczx-7-nsh), and Shandong Provincial Key Medical and Health Discipline of Oral Medicine (2024-2026). The authors also thank the "Advanced Biomaterials and Regenerative Medicine (ABRM)" Innovation Team supported by the Young-Talent Introduction and Cultivation Plan in the Universities of Shandong Province.

Author Contributions Renjie Chen: Methodology, investigation, formal analysis, data curation, software, writing—original draft. Yuanfei Wang: Methodology, formal analysis, writing—review and editing. Chenghao Yu: Methodology, investigation. Xiaopei Zhang: Methodology, software. Yawen Wang: Investigation. Tengbo Yu: Resources, supervision, funding acquisition, project administration. Tong Wu: Conceptualization, project administration, resources, supervision, funding acquisition, writing—review and editing.

Data Availability The data that support the findings of this study are available from the corresponding author upon reasonable request.

Declarations

Conflict of interest Tong Wu is an editorial board member for *Adv. Fiber Mater.*, and was not involved in the editorial review or the decision to publish this article. All authors declare that there are no competing interests.

References

1. Du D, Asaoka T, Ushida T, Furukawa KS. Fabrication and perfusion culture of anatomically shaped artificial bone using stereolithography. *Biofabrication*. **2014**;*6*:045002.
2. Cai X, Follet H, Peralta L, Gardegaront M, Farlay D, Gauthier R, Yu B, Gineyts E, Olivier C, Langer M, Gourrier A, Mitton D, Peyrin F, Grimal Q, Laugier P. Anisotropic elastic properties of human femoral cortical bone and relationships with composition and microstructure in elderly. *Acta Biomater*. **2019**;*90*:254.
3. Dekker TJ, Aman ZS, Peebles LA, Storaci HW, Chahla J, Millett PJ, Provencher MT. Quantitative and qualitative analyses of the glenohumeral ligaments: an anatomic study. *Am J Sports Med*. **1837**;*2020*:48.
4. Clarke B. Normal bone anatomy and physiology. *Clin J Am Soc Nephrol*. **2008**;*3*:S131.
5. Liu Y, Luo D, Wang T. Hierarchical structures of bone and bioinspired bone tissue engineering. *Small*. **2016**;*12*:4611.
6. Fonseca H, Moreira-Gonçalves D, Coriolano H-JA, Duarte JA. Bone quality: the determinants of bone strength and fragility. *Sports Med*. **2013**;*44*:37.
7. Wildemann B, Ignatius A, Leung F, Taitsman LA, Smith RM, Pesántez R, Stoddart MJ, Richards RG, Jupiter JB. Non-union bone fractures. *Nat Rev Dis Prim*. **2021**. https://doi.org/10.1038/s41572-021-00289-8.
8. Gillman CE, Jayasuriya AC. FDA-approved bone grafts and bone graft substitute devices in bone regeneration. *Mater Sci Eng C Mater Biol Appl*. **2021**;*130*:112466.
9. Sanz-Sánchez I, Sanz-Martín I, Ortiz-Vigón A, Molina A, Sanz M. Complications in bone-grafting procedures: classification and management. *Periodontol*. **2000**;*2022*(88):86.
10. Xavier JR, Thakur T, Desai P, Jaiswal MK, Sears N, Cosgriff-Hernandez E, Kaunas R, Gaharwar AK. Bioactive nanoengineered hydrogels for bone tissue engineering: a growth-factor-free approach. *ACS Nano*. **2015**;*9*:3109.
11. Hasani-Sadrabadi MM, Sarrion P, Pouraghaei S, Chau Y, Ansari S, Li S, Aghaloo T, Moshaverinia A. An engineered cell-laden adhesive hydrogel promotes craniofacial bone tissue

regeneration in rats. *Sci Transl Med*. **2020**. https://doi.org/10.1126/scitranslmed.aay6853.
12. Ingavle GC, Gionet-Gonzales M, Vorwald CE, Bohannon LK, Clark K, Galuppo LD, Leach JK. Injectable mineralized microsphere-loaded composite hydrogels for bone repair in a sheep bone defect model. *Biomaterials*. **2019**;*197*:119.
13. Wang L, Stegemann JP. Thermogelling chitosan and collagen composite hydrogels initiated with β-glycerophosphate for bone tissue engineering. *Biomaterials*. **2010**;*31*:3976.
14. Zhao Y, Cui Z, Liu B, Xiang J, Qiu D, Tian Y, Qu X, Yang Z. An injectable strong hydrogel for bone reconstruction. *Adv Healthc Mater*. **2019**. https://doi.org/10.1002/adhm.201900709.
15. Zhou Y, Gu Z, Liu J, Huang K, Liu G, Wu J. Arginine based poly (ester amide)/ hyaluronic acid hybrid hydrogels for bone tissue Engineering. *Carbohydr Polym*. **2020**;*230*:115640.
16. Pobloth AM, Checa S, Razi H, Petersen A, Weaver JC, Schmidt-Bleek K, Windolf M, Tatai A, Roth CP, Schaser KD, Duda GN, Schwabe P. Mechanobiologically optimized 3D titanium-mesh scaffolds enhance bone regeneration in critical segmental defects in sheep. *Sci Transl Med*. **2018**. https://doi.org/10.1126/scitranslmed.aam8828.
17. Haugen HJ, Monjo M, Rubert M, Verket A, Lyngstadaas SP, Ellingsen JE, Rønold HJ, Wohlfahrt JC. Porous ceramic titanium dioxide scaffolds promote bone formation in rabbit peri-implant cortical defect model. *Acta Biomater*. **2013**;*9*:5390.
18. He J, Fang J, Wei P, Li Y, Guo H, Mei Q, Ren F. Cancellous bone-like porous Fe@Zn scaffolds with core-shell-structured skeletons for biodegradable bone implants. *Acta Biomater*. **2021**;*121*:665.
19. Wang X, Xu S, Zhou S, Xu W, Leary M, Choong P, Qian M, Brandt M, Xie YM. Topological design and additive manufacturing of porous metals for bone scaffolds and orthopaedic implants: a review. *Biomaterials*. **2016**;*83*:127.
20. Zhao D, Yu K, Sun T, Jing X, Wan Y, Chen K, Gao H, Wang Y, Chen L, Guo X, Wei Q. Material-structure-function integrated additive manufacturing of degradable metallic bone implants for load-bearing applications. *Adv Funct Mater*. **2023**. https://doi.org/10.1002/adfm.202213128.
21. Feng G, Zhang Z, Dang M, Rambhia KJ, Ma PX. Nanofibrous spongy microspheres to deliver rabbit mesenchymal stem cells and anti-miR-199a to regenerate nucleus pulposus and prevent calcification. *Biomaterials*. **2020**;*256*:120213.
22. Mlaren JS, Macri-Pellizzeri L, Hossain KMZ, Patel U, Grant DM, Scammell BE, Ahmed I, Sottile V. Porous phosphate-based glass microspheres show biocompatibility, tissue infiltration, and osteogenic onset in an ovine bone defect model. *ACS Appl Mater Interfaces*. **2019**;*11*:15436.
23. Zhang W, Wang X, Li X, Zhang L, Jiang F. A 3D porous microsphere with multistage structure and component based on bacterial cellulose and collagen for bone tissue engineering. *Carbohydr Polym*. **2020**;*236*:116043.
24. Li J, Baker BA, Mou X, Ren N, Qiu J, Boughton RI, Liu H. Biopolymer/calcium phosphate scaffolds for bone tissue engineering. *Adv Healthc Mater*. **2013**;*3*:469.
25. Li Y, Xiao L, Wei D, Liu S, Zhang Z, Lian R, Wang L, Chen Y, Jiang J, Xiao Y, Liu C, Li Y, Zhao J. Injectable biomimetic hydrogel guided functional bone regeneration by adapting material degradation to tissue healing. *Adv Funct Mater*. **2023**. https://doi.org/10.1002/adfm.202213047.
26. Ji W, Yang F, Ma J, Bouma MJ, Boerman OC, Chen Z, van den Beucken JJJP, Jansen JA. Incorporation of stromal cell-derived factor-1α in PCL/gelatin electrospun membranes for guided bone regeneration. *Biomaterials*. **2013**;*34*:735.
27. Li C, Zhang W, Nie Y, Jiang D, Jia J, Zhang W, Li L, Yao Z, Qin L, Lai Y. Integrated and bifunctional bilayer 3D printing scaffold for osteochondral defect repair. *Adv Funct Mater*. **2023**. https://doi.org/10.1002/adfm.202214158.
28. Seyednejad H, Gawlitta D, Kuiper RV, de Bruin A, van Nostrum CF, Vermonden T, Dhert WJA, Hennink WE. In vivo biocompatibility and biodegradation of 3D-printed porous scaffolds based on a hydroxyl-functionalized poly(ε-caprolactone). *Biomaterials*. **2012**;*33*:4309.
29. Yeo M, Kim G. Nano/microscale topographically designed alginate/PCL scaffolds for inducing myoblast alignment and myogenic differentiation. *Carbohydr Polym*. **2019**;*223*:115041.
30. Liu N, Zhou Z, Ning X, Zhang X, Guo Q, Guo M, Wang Y, Wu T. Enhancing the paracrine effects of adipose stem cells using nanofiber-based meshes prepared by light-welding for accelerating wound healing. *Mater Des*. **2023**;*225*:111582.
31. El-Rashidy AA, Roether JA, Harhaus L, Kneser U, Boccaccini AR. Regenerating bone with bioactive glass scaffolds: a review of in vivo studies in bone defect models. *Acta Biomater*. **2017**;*62*:1.
32. Hohenbild F, Arango Ospina M, Schmitz SI, Moghaddam A, Boccaccini AR, Westhauser F. An in vitro evaluation of the biological and osteogenic properties of magnesium-doped bioactive glasses for application in bone tissue engineering. *Int J Mol Sci*. **2021**;*22*:12703.
33. Jeyachandran D, Murshed M, Haglund L, Cerruti M. A bioglass-poly(lactic-co-glycolic acid) scaffold@fibrin hydrogel construct to support endochondral bone formation. *Adv Healthc Mater*. **2023**. https://doi.org/10.1002/adhm.202300211.
34. Khoshakhlagh P, Rabiee SM, Kiaee G, Heidari P, Miri AK, Moradi R, Moztarzadeh F, Ravarian R. Development and characterization of a bioglass/chitosan composite as an injectable bone substitute. *Carbohydr Polym*. **2017**;*157*:1261.
35. Chang B, Liu X. Osteon: structure, turnover, and regeneration. *Tissue Eng Part B*. **2022**;*28*:261.
36. Müller R. Hierarchical microimaging of bone structure and function. *Nat Rev Rheumatol*. **2009**;*5*:373.
37. Reznikov N, Shahar R, Weiner S. Bone hierarchical structure in three dimensions. *Acta Biomater*. **2014**;*10*:3815.
38. van der Meijden RHM, Daviran D, Rutten L, Walboomers XF, Macías-Sánchez E, Sommerdijk N, Akiva A. A 3D cell-free bone model shows collagen mineralization is driven and controlled by the matrix. *Adv Funct Mater*. **2023**. https://doi.org/10.1002/adfm.202212339.
39. Li Z, Zhang S, Chen Y, Ling H, Zhao L, Luo G, Wang X, Hartel MC, Liu H, Xue Y, Haghniaz R, Lee K, Sun W, Kim H, Lee J, Zhao Y, Zhao Y, Emaminejad S, Ahadian S, Ashammakhi N, Dokmeci MR, Jiang Z, Khademhosseini A. Gelatin methacryloyl-based tactile sensors for medical wearables. *Adv Funct Mater*. **2020**. https://doi.org/10.1002/adfm.202003601.
40. Wu H, Shang Y, Sun W, Ouyang X, Zhou W, Lu J, Yang S, Wei W, Yao X, Wang X, Zhang X, Chen Y, He Q, Yang Z, Ouyang H. Seamless and early gap healing of osteochondral defects by autologous mosaicplasty combined with bioactive supramolecular nanofiber-enabled gelatin methacryloyl (BSN-GelMA) hydrogel. *Bioact Mater*. **2023**;*19*:88.
41. Chen S, Han X, Cao Y, Yi W, Zhu Y, Ding X, Li K, Shen J, Cui W, Bai D. Spatiotemporalized hydrogel microspheres promote vascularized osteogenesis via ultrasound oxygen delivery. *Adv Funct Mater*. **2023**. https://doi.org/10.1002/adfm.202308205.
42. Zhao Z, Li G, Ruan H, Chen K, Cai Z, Lu G, Li R, Deng L, Cai M, Cui W. Capturing magnesium ions via microfluidic hydrogel microspheres for promoting cancellous bone regeneration. *ACS Nano*. **2021**;*15*:13041.
43. Sutthavas P, Tahmasebi Birgani Z, Habibovic P, van Rijt S. Calcium phosphate-coated and strontium-incorporated mesoporous silica nanoparticles can effectively induce osteogenic stem cell differentiation. *Adv Healthc Mater*. **2021**. https://doi.org/10.1002/adhm.202101588.

44. Liu Y, Guo Q, Zhang X, Wang Y, Mo X, Wu T. Progress in electrospun fibers for manipulating cell behaviors. *Adv Fiber Mater*. **2023**;*5*:1241.
45. Cai B, Lin D, Li Y, Wang L, Xie J, Dai T, Liu F, Tang M, Tian L, Yuan Y, Kong L, Shen SGF. N2-polarized neutrophils guide bone mesenchymal stem cell recruitment and initiate bone regeneration: a missing piece of the bone regeneration puzzle. *Adv Sci*. **2021**. https://doi.org/10.1002/advs.202100584.
46. Wu P, Shen L, Liu H, Zou X, Zhao J, Huang Y, Zhu Y, Li Z, Xu C, Luo L, Luo Z, Wu M, Cai L, Li X, Wang Z. The marriage of immunomodulatory, angiogenic, and osteogenic capabilities in a piezoelectric hydrogel tissue engineering scaffold for military medicine. *Mil Med Res*. **2023**;*10*:35.
47. Yu C, Wang T, Diao H, Liu N, Zhang Y, Jiang H, Zhao P, Shan Z, Sun Z, Wu T, Mo X, Yu T. Photothermal-triggered structural change of nanofiber scaffold integrating with graded mineralization to promote tendon-bone healing. *Adv Fiber Mater*. **2022**;*4*:908.
48. Li L, Hao R, Qin J, Song J, Chen X, Rao F, Zhai J, Zhao Y, Zhang L, Xue J. Electrospun fibers control drug delivery for tissue regeneration and cancer therapy. *Adv Fiber Mater*. **2022**;*4*:1375.
49. Sahvieh S, Oryan A, Hassanajili S, Kamali A. Role of bone 1stem cell-seeded 3D polylactic acid/polycaprolactone/hydroxyapatite scaffold on a critical-sized radial bone defect in rat. *Cell Tissue Res*. **2020**;*383*:735.